



Crystallization and spectroscopic properties investigations of Er^{3+} doped transparent glass ceramics containing CaF_2

Zhongjian Hu, Yuansheng Wang*, En Ma, Feng Bao, Yunlong Yu, Daqin Chen

The State Key Laboratory of Structural Chemistry, Fujian Institute of Research on the Structure of Matter, Graduate School of Chinese Academy of Sciences, Chinese Academy of Sciences, Yangqiao West Road 155#, Fuzhou 350002, PR China

Received 5 January 2005; received in revised form 30 April 2005; accepted 8 July 2005

Available online 1 August 2005

Abstract

Transparent oxyfluoride glass ceramics with composition of $45\text{SiO}_2\text{--}25\text{Al}_2\text{O}_3\text{--}5\text{CaCO}_3\text{--}10\text{NaF}\text{--}15\text{CaF}_2\text{--}0.5\text{ErF}_3$ (in mol%) were developed through controlled crystallization of melt-quenched glass. Non-isothermal crystallization kinetics investigation showed that the average apparent activation energy E_a and Avrami exponent n are about 283 kJ/mol and 2.22, respectively, indicating the crystallization a three dimensional crystal growth process controlled by the diffusion with a decreasing nucleation rate. X-ray diffraction (XRD) analysis and transmission electron microscopy (TEM) observation revealed the precipitation of CaF_2 crystallites sized about 15 nm among the glass matrix after heat-treatment at 650 °C for 2 h. For as-made glass, no upconversion signals were detected when excited with a 30 mW diode laser at 980 nm, while strong upconversion emissions at 545, 660 and 800 nm were obtained for transparent glass ceramic under similar excitation condition.

© 2005 Elsevier Ltd. All rights reserved.

Keywords: A. Glasses; A. Optical materials; D. Microstructure; D. Optical properties

1. Introduction

Since rare-earth doped oxyfluoride glass ceramics were first reported by Wang and Ohwaki [1], they have attracted intensive attention due to their promising applications as upconversion fibers, optical amplifiers, solid-state lasers and 3D displays [1–3]. In such materials the rare-earth ions could

* Corresponding author. Tel.: +86 591 8370 5402; fax: +86 591 8370 5402.

E-mail address: ywang@fjirsm.ac.cn (Y. Wang).

incorporate into the crystalline phase, thus offering, for rare-earth ions, the ordered crystalline environment, which is important to reduce the multiphonon deexcitation and increase the cross-section of rare-earth ions. Evidently, rare-earth doped oxyfluoride glass ceramics may combine the optical properties of rare-earth ions in fluoride environment with the elaboration and manipulation advantage of oxide glasses [4].

Previous investigations have revealed that rare-earth ions have a strong tendency to incorporate into crystals with fluorite-type structure [5]. Glass ceramics containing PbF_2 were investigated intensively [6–9] after the system containing (Pb, Cd) F_2 nanocrystals with fluorite-type structure were developed [1]. Recently, Fu et al. [10] and Itoh et al. [11] had successively reported Eu_2O_3 doped transparent oxyfluoride glass ceramics containing CaF_2 . Erbium ion (Er^{3+}), as one of the most popular and efficient rare-earth ions, has attracted great interest due to its use for the upconversion laser and optical amplifiers [12]. The spectroscopic performances of glass ceramics are closely related to its microstructures, which are formed mainly during the course of crystallization. In present work, the crystallization behavior and kinetics, and, spectroscopic properties of a new system with the composition of $\text{SiO}_2\text{--Al}_2\text{O}_3\text{--CaCO}_3\text{--CaF}_2\text{--NaF--ErF}_3$ were investigated. To our knowledge, no similar work has been published concerning this newly developed glass ceramics system so far.

2. Experimental

The samples were prepared with the following composition (in mol%): $45\text{SiO}_2\text{--}25\text{Al}_2\text{O}_3\text{--}(15 - x)\text{CaCO}_3\text{--}x\text{NaF--}15\text{CaF}_2\text{--}0.5\text{ErF}_3$ ($x = 0.10$). For each batch, about 20 g of starting material were fully mixed and melted in a covered platinum crucible in air atmosphere at $1350\text{ }^\circ\text{C}$ for 1.5 h, and then cast into a brass mold followed by annealing at $100\text{ }^\circ\text{C}$ below the glass transition temperature (T_g) determined by differential thermal analysis (DTA) to relinquish the inner stress. The as-made sample were then heat-treated at $650\text{ }^\circ\text{C}$ for 2 h to carry out crystallization.

To identify the crystallization phase and determine the mean crystallite size, XRD was carried out with a powder diffractometer (RIGAKU-DMAX2500), using Cu $\text{K}\alpha$ radiation ($\lambda = 1.54056\text{ \AA}$), at 40 kV and 100 mA. The 2θ scan range was $5\text{--}85^\circ$, with a step size of 0.05° and a resolution of 0.01° . The microstructures of the samples were studied using a transmission electron microscope (JEM-2010) equipped with CCD system and operated at 200 kV.

The emission spectra were measured with 980 nm excitation light from 450 W Xenone lamp. By using an InP/InGaAs photomultiplier tubes (PMT) detector (R5509) the infrared luminescence signals through the emission monochromator (M300) were detected. The visible upconversion fluorescence signals were detected with a PMT detector (R928) when excited with a 30 mW diode laser at 980 nm. All the measurements were carried out at room temperature.

3. Results

3.1. Crystallization behavior

Typical DTA curves of the samples are shown in Fig. 1. There is no detectable thermal effect in the temperature DTA range of $300\text{--}800\text{ }^\circ\text{C}$ for the sample without NaF. However, DTA curve for the sample with

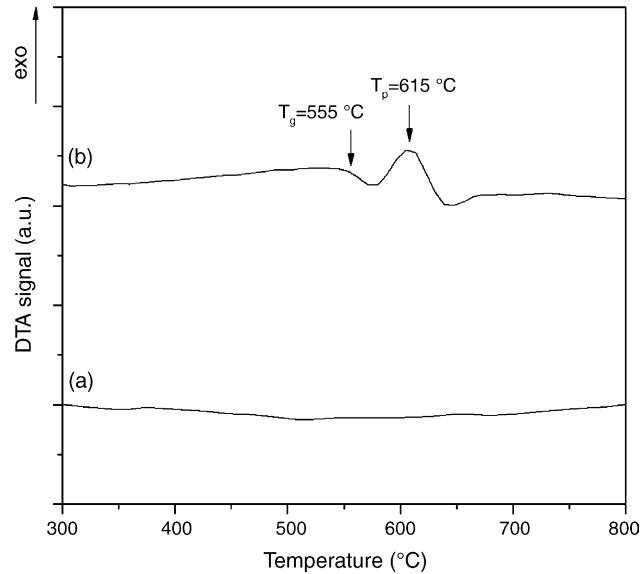


Fig. 1. DTA curves of the glass with the composition of $45\text{SiO}_2\text{-}25\text{Al}_2\text{O}_3\text{-(}15-x\text{)CaCO}_3\text{-}x\text{NaF-}15\text{CaF}_2\text{-}0.5\text{ErF}_3$ (in mol%): (a) $x = 0$; (b) $x = 10$.

10% NaF presents a unique exothermal peak at about 615°C . XRD results presented in Fig. 2 exhibit that only a diffuse hump appears for the as-made sample evidencing the amorphous nature of the structure, while several sharp CaF_2 diffraction peaks emerge for the sample heat-treated at 650°C , which reveals that the exothermal peak is attributed to the crystallization of CaF_2 phase. From the XRD peaks width and Scherrer equation, the mean size of CaF_2 crystallites was estimated to be about 15 nm. In Fig. 3, TEM

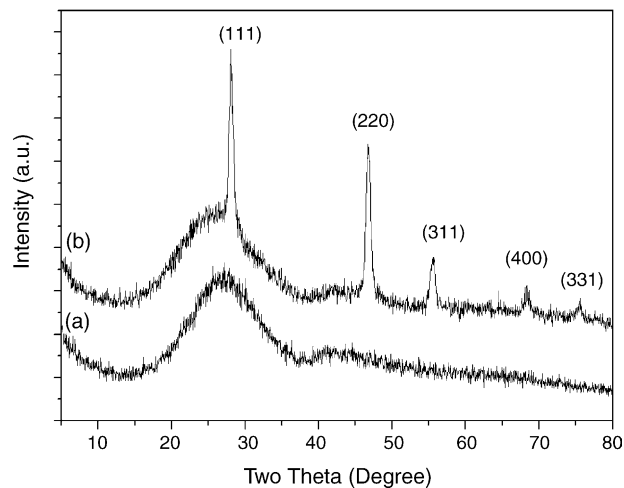


Fig. 2. XRD patterns of sample with 10% NaF: (a) as-made; (b) heat-treated at 650°C for 2 h.

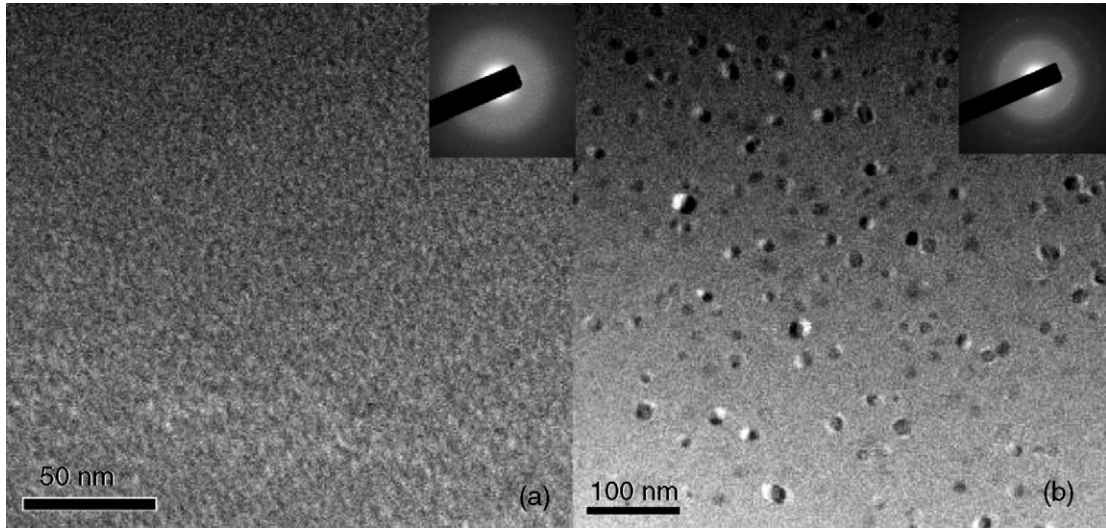


Fig. 3. TEM bright field images and corresponding electron diffraction patterns of sample with 10% NaF: (a) as-made; (b) heat-treated at 650 °C for 2 h.

micrograph for the as-made sample presents a uniform contrast, while for the glass ceramic lots of spherical CaF_2 crystallites sized about 15–20 nm are distributed separately and homogeneously among the glassy matrix, in good accordance with the XRD results.

3.2. Crystallization kinetics

The non-isothermal method has been used to determine the crystallization kinetics. The apparent activation energy E_a and the Avrami exponent n , two most important kinetic parameters for crystallization, can be obtained from DTA results using the equations proposed by Chen [13] and Ozawa [14,15]

$$\text{Chen's equation : } \frac{d[\ln(T_p^2/\alpha)]}{d(1/T_p)} = \frac{E_a}{R} \quad (1)$$

$$\text{Ozawa's equation : } \frac{d(\ln \alpha)}{d(1/T_p)} = -\frac{E_a}{R} \quad (2)$$

$$\text{Ozawa's equation : } \left. \frac{d\{\ln[-\ln(1-x)]\}}{d \ln \alpha} \right|_{T_x} = -n \quad (3)$$

where α is the heating rate, T_p the crystallization temperature at a given heating rate, E_a the apparent activation energy for crystallization, R the gas constant, n the Avrami exponent and x the crystallized volume fraction at a fixed temperature T_x with the heating rate α . Pieces of bulk sample were subjected to DTA analysis at different heating rates of 10, 15, 20 and 25 K/min, respectively.

From the slopes of the two plots in Fig. 4, the values of E_a were estimated to be 275 kJ/mol for Chen's method and 290 kJ/mol for Ozawa's method, respectively. According to the data from DTA

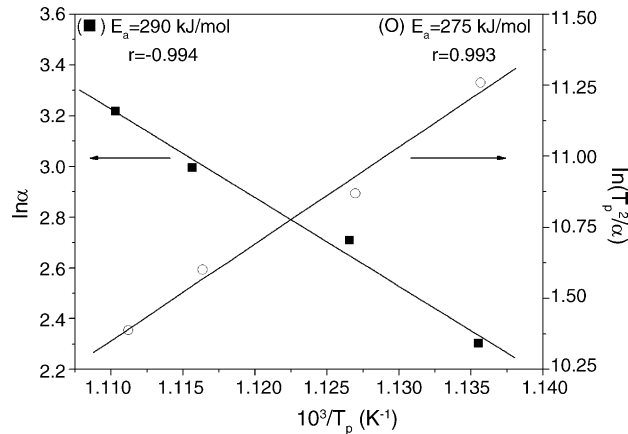


Fig. 4. Determination of the apparent activation energy E_a ((■) Ozawa's method; (○) Chen's method). r is the correlative coefficient of least-squares fitting.

measurements and Eq. (3), the plots of $\ln[-\ln(1-x)]$ versus $\ln \alpha$ are shown in Fig. 5. The values of the Avrami exponent n , determined from the slopes of these plots, are also presented. The average value of n is 2.22.

3.3. Spectroscopic properties

Fig. 6 shows the Er^{3+} emission spectra of ${}^4\text{I}_{13/2} \rightarrow {}^4\text{I}_{15/2}$ transition obtained under 980 nm excitation. Inhomogeneously broadened spectrum expected for amorphous host is observed for the as-made glass. For heat-treated sample this spectrum slightly splits, and a new maximum appears at about 1545 nm.

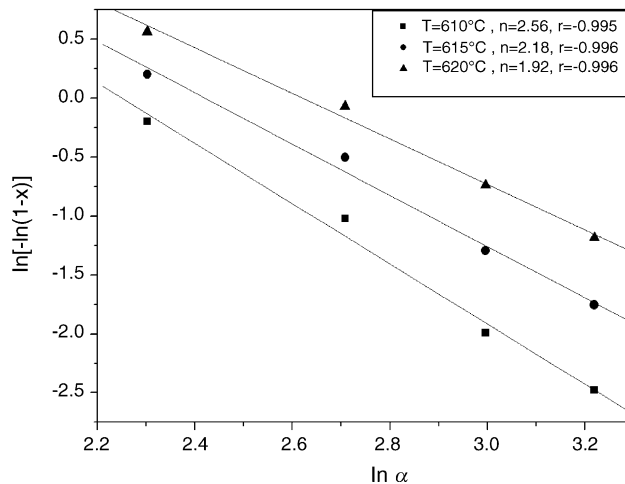


Fig. 5. Determination of the Avrami exponent n by Ozawa's method. r is the correlative coefficient of least-squares fitting.

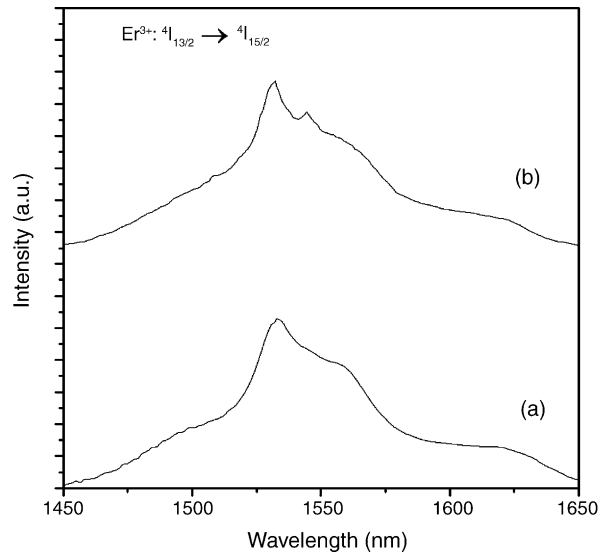


Fig. 6. Emission spectra for the sample with 10% NaF excited at 980 nm: (a) as-made; (b) heat-treated at 650 °C for 2 h.

Fig. 7 exhibits a well-resolved upconversion spectrum with narrow emission lines of the glass ceramic sample in the wavelength range of 500–850 nm excited at 980 nm. Three emissions at 545, 660 and 800 nm are observed, which are due to ${}^4S_{3/2}({}^2H_{11/2}) \rightarrow {}^4I_{15/2}$, ${}^4F_{9/2} \rightarrow {}^4I_{15/2}$ and ${}^4S_{3/2}({}^2H_{11/2}) \rightarrow {}^4I_{13/2}$ transitions, respectively. The red emission peaked at 660 nm is very strong, being easily detected with naked eye when excited with a 30 mW diode laser. As the comparison, no upconversion signals for the as-made glass under the same excitation condition had been detected.

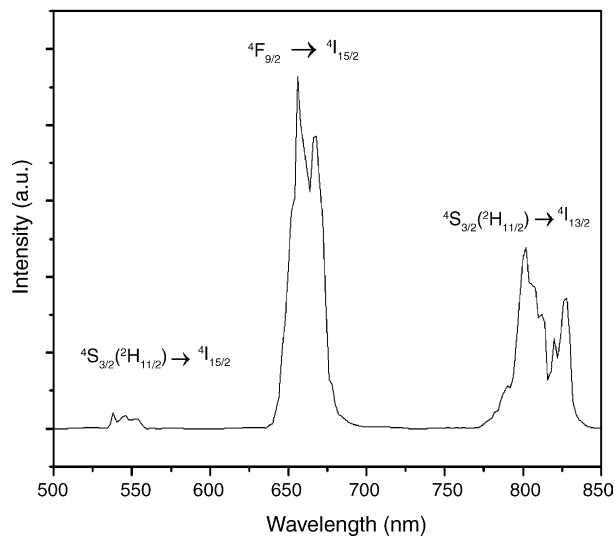


Fig. 7. Upconversion emission spectrum for the glass ceramic excited with a 30 mW diode laser at 980 nm.

4. Discussion

For fabricating oxyfluoride glass ceramics a main drawback is the irreproducibility in stoichiometry due to the fluoride loss during melting [16]. In order to obtain desired oxyfluoride glass ceramics, the as-made glass should contain near stoichiometric fluoride. In present work, CaF_2 crystallites would not precipitate from the glass matrix when only 15% CaF_2 was added to the raw material as the fluorine source. When 10% NaF was further added, CaF_2 crystallites easily precipitated after appropriate heat-treatment. Obviously, the addition of NaF, to some extent, compensates the fluorine loss during melting.

The average crystallization apparent activation energy E_a of 283 kJ/mol and the Avrami parameters of 2.22 indicate the crystallization mechanism a three-dimensional crystal growth process controlled by the diffusion with a decreasing nucleation rate [17,18]. According to the previous work [6], Er^{3+} may acts as the nucleation agent during crystallization in oxyfluoride glass. Thus, the number of the nucleation center probably reaches a maximum amount at the beginning of crystallization, and it decreases markedly with the proceeding of crystallization when neglecting those caused by the thermal fluctuation in the system.

The good transparency of glass ceramic, which is ascribed to weak light scattering as a result of the smallness of the nanosized crystallites with respect to the wavelength of visible light, provides a prerequisite condition for spectroscopic measurements. The 1.53 μm emission peak splitting of glass ceramic is considered to be due to the site transition of Er^{3+} ions from a glass-like environment to a crystal-like one. The multiphonon relaxation rate of upconverted emissions is very sensitive to the phonon energy of the host matrix and, thus, efficient upconversion is observed primarily in matrices with phonon of low cut-off energy (below 1000 cm^{-1}) [19,20]. In the as-made glass sample, Er^{3+} ions are randomly dispersed among the oxyfluoride glassy matrix, the phonon energy of which is so large that the effective upconversion emission is prohibited. For the glass ceramic sample, the emergence of strong upconversion emissions at the visible and near-infrared wavelengths when excited with a pump power of 30 mW implies that Er^{3+} ions are mostly confined in a fluoride crystalline environment which, with low phonon energy (generally lower than 500 cm^{-1}), reduces the non-radiative loss due to multiphonon relaxation and thus yields strong upconversion signals [21]. The upconversion performance of present glass ceramic is similar to that of CaF_2 single crystal with the same Er^{3+} doping level reported by Joutart and Oomen [22], in which intense red upconversion was also obtained.

5. Conclusion

A new ErF_3 doped transparent glass ceramic containing CaF_2 crystals had been fabricated. After appropriate heat-treatment, nanosized spherical CaF_2 crystallites precipitated separately and homogeneously among the glassy matrix. The kinetics analysis indicated the crystallization mechanism a three-dimensional crystal growth process controlled by the diffusion with a decreasing nucleation rate. For glass ceramic, compared with the as-made glass, the 1.53 μm emission band of Er^{3+} split slightly and a new maximum appeared at about 1545 nm under 980 nm excitation. Besides, when excited with a 30 mW diode laser, upconversion luminescence at 545, 800 nm and especially very strong at 660 nm was obtained, which was similar to the case for Er^{3+} doped CaF_2 single crystal, revealing that Er^{3+} ions have been incorporated into the fluoride crystalline phase.

Acknowledgements

This work was supported by grants from the Natural Science Foundation of Fujian Province China (Project No. A0320001), the Ministry of Science and Technology of China (Project No. 2003BA323C) and the State Key Laboratory of Structural Chemistry (Project No. 050005).

References

- [1] Y. Wang, J. Ohwaki, *Appl. Phys. Lett.* 63 (1993) 3268.
- [2] P.A. Tick, N.F. Borrelli, L.K. Cornelius, M.A. Newhouse, *J. Appl. Phys.* 78 (1995) 93.
- [3] M.J. Dejneka, *MRS Bull.* 23 (1998) 57.
- [4] X. Qiao, X. Fan, M. Wang, X. Zhang, *Opt. Mater.* 27 (2004) 597.
- [5] K. Hirao, Y. Benino, T. Komatsu, *J. Phys. Chem. Solids* 62 (2001) 2079.
- [6] M. Mortier, F. Auzel, *J. Non-Cryst. Solids* 256–257 (1999) 361–365.
- [7] M. Mortier, P. Goldner, C. Chateau, M. Genotelle, *J. Alloys Comp.* 323–324 (2001) 753–758.
- [8] A.S. Gouveia-Neto, E.B. da Costa, L.A. Bueno, S.J.L. Ribeiro, *J. Lumin.* 110 (2004) 79–84.
- [9] L.L. Kukkonen, I.M. Reaney, D. Furniss, M.G. Pellatt, A.B. Seddon, *J. Non-Cryst. Solids* 290 (2001) 25–31.
- [10] J. Fu, J.M. Parker, P.S. Flower, R.M. Brown, *MRS Bull.* 37 (2002) 1843.
- [11] M. Itoh, T. Sakurai, T. Yamakami, J. Fu, *J. Lumin.* 112 (2005) 161–165.
- [12] J. Yang, L. Zhang, L. Wen, S. Dai, L. Hu, Z. Jiang, *J. Appl. Phys.* 95 (2004) 3020.
- [13] H.S. Chen, *J. Non-Cryst. Solids* 27 (1978) 257.
- [14] T. Ozawa, *Polymer* 12 (1971) 150.
- [15] T. Ozawa, *Polymer* 12 (1971) 150–158.
- [16] L.A. Bueno, P. Melnikov, Y. Messaddeq, S.J.L. Ribeiro, *J. Non-Cryst. Solids* 247 (1999) 87–91.
- [17] M. Poulain, *J. Non-Cryst. Solids* 184 (1995) 103.
- [18] M. Matecki, I. Noiret-Chiaruttini, J. Lucas, *J. Non-Cryst. Solids* 127 (1991) 136.
- [19] L. Eatenkamp, G.F. West, J. Tobben, *J. Non-Cryst. Solids* 140 (1992) 35.
- [20] A. Biswas, G.S. Maciel, C.S. Friend, P.N. Prasad, *J. Non-Cryst. Solids* 316 (2003) 395.
- [21] K. Hirao, S. Kishimoto, K. Tanaka, S. Tanabe, N. Soga, *J. Non-Cryst. Solids* 139 (1992) 151.
- [22] J.P. Jouart, E.W.J. Oomen, *Phys. Stat. Sol. (b)* 172 (1992) 468.